Inorg. Chem. **2008**, *47*, 9848−9856

Axial Ligand Coordination in Sterically Strained Vanadyl Porphyrins: Synthesis, Structure, and Properties

Sudip Kumar Ghosh, Ranjan Patra, and Sankar Prasad Rath*

Department of Chemistry, Indian Institute of Technology, Kanpur 208016, India

Received April 22, 2008

A hitherto unknown family of six-coordinate vanadyl porphyrins of the sterically crowded, nonplanar 2,3,7,8,12,13,17,18-octaethyl-5,10,15,20-tetranitroporphyrin incorporating axial ligand L [where L is pyridine, tetrahydrofuran (THF), or methanol (MeOH)] has been isolated as VO(*tn*-OEP)(L) in the solid phase for the first time and also structurally characterized. The presence of four electron-withdrawing, bulky nitro groups at the meso positions of vanadyl octaethylporphyrins severely distorts the porphyrin macrocycles and significantly enhances the affinity for the axial ligands, where even weak σ-donating ligands, such as MeOH, bind strongly enough to be isolable in the solid phase and that too under the offset effects of the macrocyclic distortions. Thus, the axial ligand affinity is influenced by both the electronic and conformational effect, which cannot be separated completely in this series. The solid-state magnetic measurements and their typical electron paramagnetic resonance (EPR) spectrum show the presence of a single, unpaired electron, consistent with V(IV) formulation. The V═O stretching frequency for VO(*tn*-OEP) occurs as a sharp, strong peak at 1008 cm^{-1}, which is consistent with five-coordinate vanadyl porphyrins, while VO(*tn*-OEP)(L) displays a strong band at lower wavenumbers. The downshift in ν(V═O) upon axial coordination increases with increasing donor strength of the axial ligands; for pyridine, the downshift is 30 cm^{-1}, while for THF and MeOH, the downshifts are nearly 18 cm^{-1}. X-ray structure determinations authenticate axial coordination in a purely saddle-distorted porphyrin macrocycle for all of the complexes reported here in which V−Np distances are significantly shorter, while the porphyrin cores have been expanded on axial ligand coordination. As a result, vanadium atoms are more inplane than in a five-coordinate species. The binding of L does not change the spin or metal oxidation states (V^{IV}, d^1-system) of the complexes; therefore, the changes observed are truly the reflections of axial ligand coordination. Electrochemical data obtained from cyclic voltammetric studies reveal that the complexes are much easier to reduce (by ∼1200 mV) but more difficult to oxidize (by ∼500 mV) as compared to nearly planar VO(OEP). The complexes undergo two one-electron oxidations due to π-cation radical and dication formation and three one-electron reductions. The first two reductions are because of π-anion radical and dianion formation, while the third quasi-reversible reduction is assigned to a metal-centered process ($V^{IV} \rightarrow V^{III}$). These results can be useful for identifying the interaction of the vanadyl porphyrins with the biological targets in their reported involvement in potent insulinomimetic activity and in anti-HIV agents.

Introduction

Vanadium is a physiologically essential element, and its concentration in human serum is about 100 ng/L.[1] Although vanadyl porphyrins are not yet known to be involved in any biological processes, they do occur in nature and are widely distributed within naturally occurring components of sediments and petroleum deposits.[2−4] Recently, vanadyl porphyrins have attracted much attention due to their reported[5,6]

* To whom correspondence should be addressed. E-mail: sprath@iitk.ac.in. Phone: +91-512-259 7251. Fax: +91-512-259 7436.

(1) Crans, D. C.; Smee, J. J.; Gaidamauskas, E.; Yang, L. *Chem. Rev.* **2004**, *104*, 849.

(2) Callot, H. J.; Ocampo, R. In *The Porphyrin Handbook*; Kadish, K. M., Smith, K. M., Guilard, R., Eds.; Academic Press: New York, 2000; Vol. 1, p 349.

(3) (a) Callot, H. J. In *The Chlorophylls*; Scheer, H., Ed.; CRC Press: Boca Raton, FL, 1991; p 339. (b) Baker, E. W.; Louda, J. W. In *Biological Markers in the Sedimentary Record*; John, R., Ed.; Elsevier: Amsterdam, 1986; p 125.

(4) (a) Czernuszewicz, R. S. *J. Porphyrins Phthalocyanines* **2000**, *4*, 426. (b) Kashiyama, Y.; Shiro, M.; Tada, R.; Ohkouchi, N. *Chem. Lett.* **2007**, *36*, 706.

10.1021/ic800714w CCC: $40.75
Published on Web 09/30/2008

involvement in potent insulinomimetic activity and also as anti-HIV agents, although the nature of the interactions with the biological targets is not known yet. However, it has been found that the porphyrin macrocycles within the protein are quite flexible and can adopt multiple nonplanar conformations, in which the extent and nature are mainly controlled by protein side chains.[7,8] These distortions have been shown to modulate the photophysical and chemical properties of the chromophores and are believed to be responsible, at least in part, for the various functions and reactivity of chemically similar tetrapyrrole pigments found in nature. The nonplanar distortions of tetrapyrroles that occur naturally in proteins can be induced in model porphyrins by substantial steric crowding at the periphery, which has led to the synthesis and structural characterization of a large number of sterically crowded porphyrins.[7−11]

This state of development has prompted us to synthesize vanadyl porphyrins that easily bind various O/N donor ligands to the sixth position, which is the only position available, and enables us to investigate the effects of axial ligand coordination. It has been known for some time that the axial ligand coordination to vanadyl porphyrins has existed in solution,[12,13] but its authentic existence in the solid state had not yet been confirmed. It also is interesting to investigate the effect of macrocycle distortions on the properties of a metal center.

Herein, we wish to report on a hitherto unknown family of vanadyl porphyrins that binds the axial ligand strongly enough to be isolable in the solid state and also to scrutinize the effect of axial ligand coordination on the electronic structure and geometry of the vanadyl centers. This objective has been achieved successfully by using 2,3,7,8,12,13,17,18-octaethyl-5,10,15,20-tetranitroporphyrins (*tn*-H_2OEP) as a porphyrin macrocycle. The presence of four electron-withdrawing, bulky nitro groups at the meso positions severely distorts the porphyrin geometry and provides an interesting modulation of the macrocycle properties that for the first time enables the facile isolation of a series of six-coordinate VO(*tn*-OEP)(L) in the solid state, even under the offset effects of the macrocycle distortions and being structurally characterized. Also, the binding of L does not change the spin or oxidation states of the metal (V^{IV}, d^1-system); therefore, the changes observed are truly the reflections of axial ligand coordination. We also investigate the effects of the macrocycle deformations on the metal centers in order to understand the effects of similar distortions in biology.

Results and Discussion

Porphyrin macrocycles can be distorted via the introduction of sterically demanding substituents in the porphyrin periphery. We have synthesized 2,3,7,8,12,13,17,18-octaethyl-5,10,15,20-tetranitroporphyrins (*tn*-H_2OEP) because of their highly nonplanar geometry, and also because the presence of four electron-withdrawing, meso nitro groups provides an interesting modulation of the macrocycle properties. The free ligand (*tn*-H_2OEP) has been synthesized via demetalation of Zn(*tn*-OEP) as reported previously,[14] and the vanadium metal is inserted by refluxing the free ligand in dimethylformamide (DMF) with $VOSO_4$ under nitrogen for nearly 2.5 h followed by chromatographic separation in neutral alumina using chloroform as eluent to form VO(*tn*-OEP) in good yields. The ultraviolet−visible (UV−vis) spectrum of the molecule shows the Soret and two Q-bands at 427, 556, and 596 nm, respectively, whereas the nearly planar VO(OEP) shows peaks at 407, 534, and 573 nm for the same bands. The observed red shift and broadening of the bands are indicative of the highly distorted porphyrins in solution.[15]

However, the addition of a small amount of pyridine to the chloroform solution of VO(*tn*-OEP) immediately red-shifted the Soret band to 435 nm and the two Q-bands to 565 and 590 nm, indicating pyridine coordination to form six-coordinate VO(*tn*-OEP)(py) in solution (Scheme 1). Figure 1 shows the gradual changes in the UV−vis spectra of VO(*tn*-OEP) in the presence of varying amounts of pyridine, where the peaks corresponding to the six-coordinate VO(*tn*-OEP)(py) at 376, 435, and 565 nm are gaining in intensity and the peaks corresponding to VO(*tn*-OEP) at 427, 556, and 596 nm are decreasing in intensity. A clean and quantitative transformation is evidenced by well-anchored isosbestic points at 386, 439, 527, 558, 581, and 615 nm.

(5) Kiss, T.; Jakusch, T.; Pessoa, J. C.; Tomaz, I. *Coord. Chem. Rev.* **2003**, *237*, 123.
(6) (a) Wong, S.-Y.; Sun, R. W.-Y.; Chung, N. P. Y.; Lin, C.-L.; Che, C.-M. *Chem. Commun. (Cambridge, U.K.)* **2005**, 3544. (b) Saha, T. K.; Adachi, Y.; Yoshikawa, Y.; Yasui, H.; Sakurai, H. *Chem. Lett.* **2005**, *34*, 1350. (c) Sakurai, H.; Inohara, T.; Adachi, Y.; Kawabe, K.; Yasuia, H.; Takada, J. *Bioorg. Med. Chem. Lett.* **2004**, *14*, 1093.
(7) Shelnutt, J. A. In *The Porphyrin Handbook*; Kadish, K. M., Smith, K. M., Guilard, R., Eds.; Academic Press: New York, 2000; Vol. 7, p 167.
(8) (a) Shelnutt, J. A.; Song, X.-Z.; Ma, J.-G.; Jia, S.-L.; Jentzen, W.; Medforth, C. J. *Chem. Soc. Rev.* **1998**, *27*, 31. (b) Gazeau, S.; Pécaut, J.; Haddad, R.; Shelnutt, J. A.; Marchon, J.-C. *Eur. J. Inorg. Chem.* **2002**, *11*, 2956. (c) Jentzen, W.; Song, X. Z.; Shelnutt, J. A. *J. Phys. Chem. B* **1997**, *101*, 1684. (d) Ravikanth, M.; Chandrashekar, T. K. *Struct. Bonding (Berlin, Ger.)* **1995**, *82*, 107.
(9) (a) Senge, M. O. In *The Porphyrin Handbook*; Kadish, K. M., Smith, K. M., Guilard, R., Eds.; Academic Press: New York, 2000; Vol. 1, p 239. (b) Senge, M. O. *Chem. Commun. (Cambridge, U.K.)* **2006**, 243.
(10) (a) Nakamura, M.; Ohgo, Y.; Ikezaki, A. *J. Inorg. Biochem.* **2008**, *102*, 433. (b) Nakamura, M. *Coord. Chem. Rev.* **2006**, *250*, 2271. (c) Walker, F. A. *Chem. Rev.* **2004**, *104*, 589. (d) Walker, F. A. *Coord. Chem. Rev.* **1999**, *186*, 471.
(11) (a) Scheidt, W. R. In *The Porphyrin Handbook*; Kadish, K. M., Smith, K. M., Guilard, R., Eds.; Academic Press: New York, 2000; Vol. 3, p 49. (b) Scheidt, W. R.; Reed, C. A. *Chem. Rev.* **1981**, *81*, 543.
(12) (a) Guilard, R.; Lecomte, C. *Coord. Chem. Rev.* **1985**, *65*, 87. (b) Walker, F. A.; Hui, E.; Walker, J. M. *J. Am. Chem. Soc.* **1975**, *97*, 2390. (c) Su, Y. O.; Czernuszewicz, R. S.; Miller, L. A.; Spiro, T. G. *J. Am. Chem. Soc.* **1988**, *110*, 4150. (d) Shelnutt, J. A.; Dobry, M. M. *J. Phys. Chem.* **1983**, *87*, 3012. (e) Czarnecki, K.; Proniewicz, L. M.; Fujii, H.; Ji, D.; Czernuszewicz, R. C.; Kincaid, J. R. *Inorg. Chem.* **1999**, *38*, 1543. (f) Doukkali, A.; Saoiabi, A.; Ferhat, M.; Mugnier, Y.; Vallat, A.; Guilard, R. *New J. Chem.* **2006**, *30*, 997.
(13) Scbulz, C. E.; Song, H.; Lee, Y. J.; Mondal, J. U.; Mohanrao, K.; Reed, C. A.; Walker, F. A.; Scheidt, W. R. *J. Am. Chem. Soc.* **1994**, *116*, 7196.
(14) Gong, L.; Dolphin, D. *Can. J. Chem.* **1985**, *63*, 401.
(15) (a) Song, Y.; Haddad, R. E.; Jia, S.-L.; Hok, S.; Olmstead, M. M.; Nurco, D. J.; Schore, N. E.; Zhang, J.; Ma, J.-G.; Smith, K. M.; Gazeau, S.; Pécaut, J.; Marchon, J.-C.; Medforth, C. J.; Shelnutt, J. A. *J. Am. Chem. Soc.* **2005**, *127*, 1179. (b) Medforth, C. J.; Senge, M. O.; Smith, K. M.; Sparks, L. D.; Shelnutt, J. A. *J. Am. Chem. Soc.* **1992**, *114*, 9859.

Scheme 1

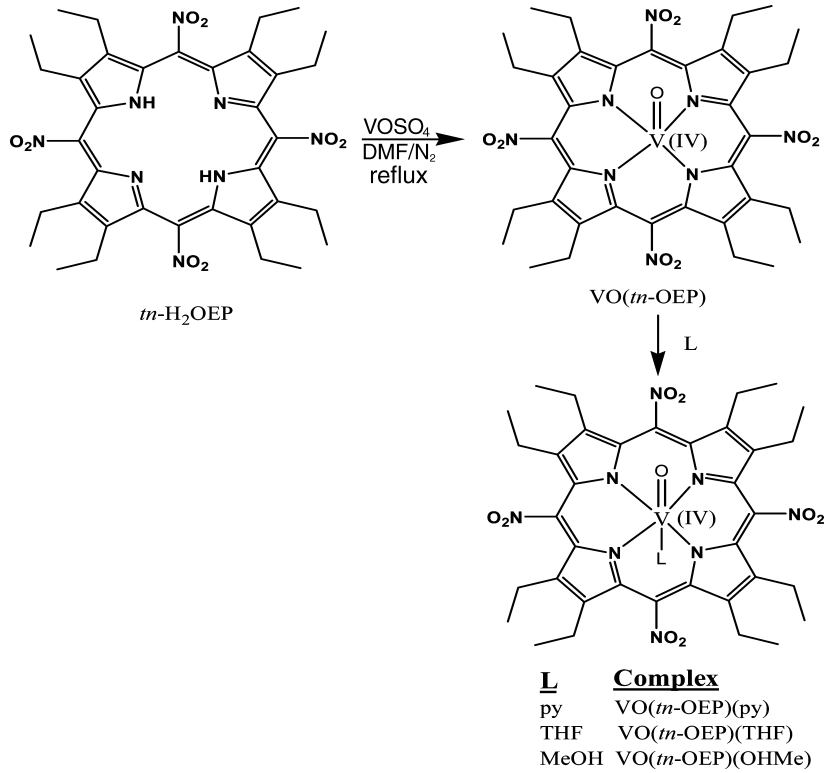

Similar observations are also obtained when using THF and MeOH as axial ligands because of the formation of VO(*tn*-OEP)(THF) and VO(*tn*-OEP)(OHMe), respectively (for UV−vis spectra, see Supporting Information, Figure S1).

All the complexes are isolated in the solid state in excellent yields and characterized using various spectroscopic techniques. The solid-state magnetic measurements at room temperature show the presence of a single, unpaired electron (μ_{eff} at 295 K, 1.71−1.80 μ_B) in each case that was further confirmed by their typical EPR spectrum with well-resolved ^{51}V hyperfine lines in both the solid and solution phases, which is consistent with V(IV) formulation, vide infra. The V═O stretch for VO(*tn*-OEP) occurs as a sharp, strong peak at 1008 cm^{-1}, which is consistent with five-coordinate vanadyl porphyrins, while the V═O stretch for VO(*tn*-OEP)(L) displays a strong band at lower wavenumbers. The downshift in ν(V═O) upon axial ligation increases with increasing donor strength of the axial ligands; for pyridine, the downshift is 30 cm^{-1}, while for THF and MeOH, the downshifts are ∼18 cm^{-1} (Experimental Section). The hydrogen-bonded methanolic OH stretch occurs as a broad peak near 3438 cm^{-1} for VO(*tn*-OEP)(OHMe). Although we are unable to obtain X-ray quality crystals for VO(*tn*-OEP), the single crystal X-ray structures of VO(*tn*-OEP)(py), VO(*tn*-OEP)(THF), and VO(*tn*-OEP)(OHMe) have been determined successfully at 100 K.

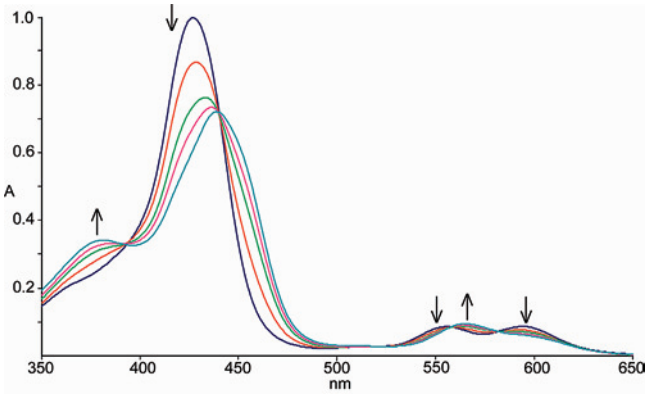

Figure 1. Spectral change of VO(*tn*-OEP) in chloroform in the presence of varying amounts of pyridine forming VO(*tn*-OEP)(py); arrows indicate an increase or decrease of band intensity.

Crystallographic Characterization of VO(*tn*-OEP)(py). Dark purple crystals were grown by slow diffusion of cyclohexane into a benzene solution of VO(*tn*-OEP) containing 5% pyridine at room temperature in the presence of air. The complex crystallizes in the orthorhombic crystal system with the *Pnma* space group, where one-half of the molecule is present in the asymmetric unit, and the vanadium atom is located at the center of symmetry. Figure 2 shows a drawing of the six-coordinate vanadyl complex; the selected inter-

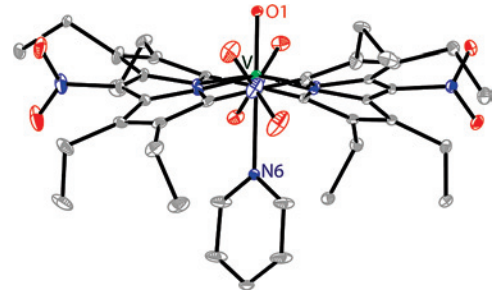

Figure 2. Perspective view for VO(*tn*-OEP)(py) showing 50% thermal contours for all non-hydrogen atoms (H atoms have been omitted for clarity).

Table 1. Selected Bond Lengths and Angles

	VO(*tn*-OEP) (py)	VO(*tn*-OEP) (OHMe)	VO(*tn*-OEP) (THF)
	Bond Lengths (Å)		
V−O1	1.600(3)	1.595(2)	1.592(3)
V−N1	2.060(3)	2.069(2)	2.081(2)
V−N2	2.075(3)	2.068(2)	2.066(3)
V−N3	2.082(2)	2.0614(2)	2.071(3)
V−N6/O6	2.492(3)	2.424(3)	2.404(3)
O2−N4	1.217(4)	1.225(3)	1.218(3)
O3−N4	1.219(4)	1.216(3)	1.223(3)
O4−N5	1.218(3)	1.222(3)	1.217(4)
O5−N5	1.224(3)	1.217(3)	1.217(4)
	Bond Angles (deg)		
O1−V−N1	99.87(13)	100.42(11)	97.40(6)
O1−V−N2	100.64(13)	102.31(11)	99.94(13)
O1−V−N3	96.92(6)	97.58(5)	100.74(13)
O1−V−N6/O6	179.53(12)	179.94(10)	179.77(11)
N1−V−N2	159.48(12)	157.27(10)	88.72(6)
N1−V−N3	88.78(6)	88.32(5)	88.63(6)
N2−V−N3	88.76(6)	88.70(5)	159.32(12)
N1−V−N6/O6	80.59(11)	79.64(9)	82.60(6)
N2−V−N6/O6	78.89(11)	77.63(9)	79.83(10)
N3−V−N6/O6	83.08(6)	82.42(5)	79.49(11)
C19−N6/O6−V	122.99(19)	126.5(11)	127.8(3)

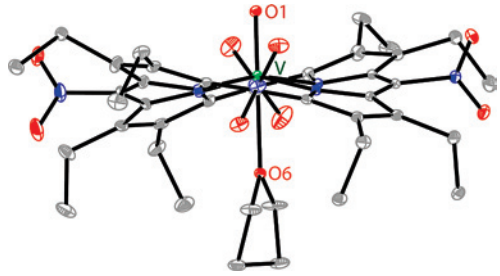

Figure 3. Perspective view for VO(*tn*-OEP)(THF) showing 50% thermal contours for all non-hydrogen atoms (H atoms have been omitted for clarity).

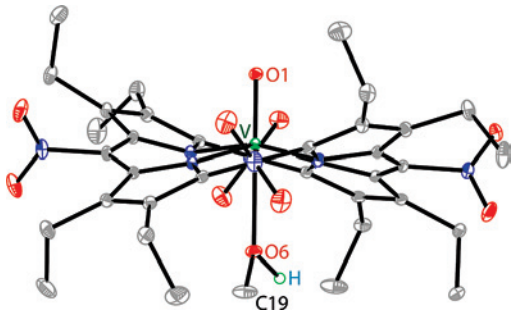

Figure 4. Perspective view for VO(*tn*-OEP)(OHMe) showing 50% thermal contours for all non-hydrogen atoms (only methanolic hydrogen is shown).

atomic distances and angles are listed in Table 1, and crystal data are shown in Table 2. In the crystal structure, the V(IV) center has a six-coordinate, distorted, octahedral geometry with the four porphyrinic nitrogen atoms on the base of the octahedron, while the oxo oxygen and axial pyridine ligands are occupying the apical sites of the octahedron. Also, the vanadium metal is displaced by 0.31 Å toward the oxo oxygen from the least-squares plane containing four porphyrinic nitrogens. The V−Np distances are in the range of 2.06−2.08 Å, while the V−N(py) distance is 2.492(3) Å, which is significantly longer because of the trans influence of the vanadyl oxo group. The axial pyridine moiety is tilted

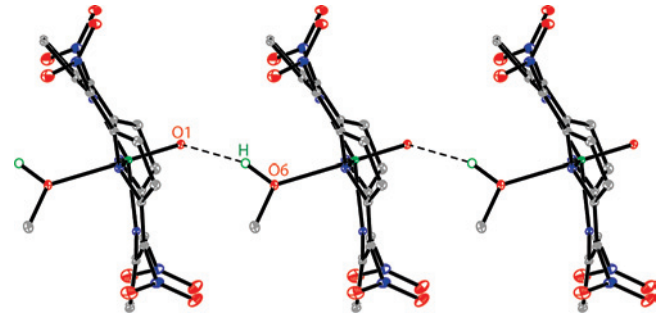

Figure 5. Hydrogen bonding interactions among the molecules in VO(*tn*-OEP)(OHMe) forming an infinite chain (ethyl group and other hydrogens have been omitted for clarity).

by 4.9° from the perpendicular of the mean porphyrin plane (24 atoms) and is nearly eclipsed with a 4.5° dihedral angle between the planes of the nearest Np−Fe−Nax and pyridine ligand.

Crystallographic Characterization of VO(*tn*-OEP)(THF). Dark purple crystals were grown by slow diffusion of cyclohexane into a THF solution of VO(*tn*-OEP) at room temperature in the presence of air. The complex also crystallizes in the same orthorhombic *Pnma* space group where one-half of the molecule is present in the asymmetric unit; Figure 3 shows the structure of the complex. Selected interatomic distances and angles are given in Table 1, and crystal data are shown in Table 2. Similar to the previous structure, the V(IV) center also has a six-coordinate distorted octahedral geometry, and the metal atom is displaced by 0.32 Å toward the oxo oxygen from the least-squares plane of four porphyrinic nitrogens. V−Np distances spread in the narrow range of 2.07−2.08 Å, and the axial V−O(THF) distance is 2.404(3) Å, which is much longer than the V−O(oxo) bond of 1.592(3) Å.

Crystallographic Characterization of VO(*tn*-OEP)(OHMe). The crystallographically determined structure of VO(*tn*-OEP)(OHMe) is shown in Figure 4. Dark purple crystals of the molecule were grown by slow diffusion of methanol into a benzene solution of VO(*tn*-OEP) at room temperature in the presence of air. The complex crystallizes in orthorhombic space group *Pnma*, where the vanadium atom is located at the center of symmetry as before. The selected bond distances and angles are compared in Table 1, and crystal data are given in Table 2.

Methanol is a ligand that is certainly not known for its strong complexing power. However, the presence of four electron-withdrawing, bulky nitro groups at the meso positions provides an interesting modulation of the macrocycle properties that enables the facile formation and isolation of VO(*tn*-OEP)(OHMe) in the solid state even in a distorted macrocyclic environment. The V(IV) center has a six-coordinate, distorted, octahedral geometry, and the metal center is displaced by 0.35 Å toward the oxo oxygen from the mean porphyrin plane (24 atoms). The V−N1, V−N2, and V−N3 distances, which are the inplane distances to the porphyrinic nitrogen atoms, are 2.069(2), 2.068(2), and 2.061(2) Å, respectively. The vanadium−oxo oxygen distance is 1.595(2) Å, while the vanadium−methanolic oxygen

Table 2. Crystal Data and Data Collection Parameters

	VO(*tn*-OEP)(py)	VO(*tn*-OEP)(OHMe)	VO(*tn*-OEP)(THF)
T (K)	100(2)	100(2)	100(2)
formula	$C_{41}H_{45}N_9O_9V$	$C_{37}H_{44}N_8O_{10}V$	$C_{40}H_{48}N_8O_{10}V$
formula weight	858.80	811.74	851.80
color and habit	dark purple	dark purple	dark purple
crystal system	orthorhombic	orthorhombic	orthorhombic
space group	*Pnma*	*Pnma*	*Pnma*
a (Å)	18.1637(16)	24.922(5)	18.3407(14)
b (Å)	22.4499(18)	23.891(5)	22.4467(16)
c (Å)	9.7448(8)	6.5645(13)	9.5934(7)
α (deg)	90	90	90
β (deg)	90	90	90
γ (deg)	90	90	90
V (Å^3)	3973.7(6)	3908.5(14)	3949.5(5)
radiation (λ, Å)	Mo Kα (0.71073)	Mo Kα (0.71073)	Mo Kα (0.71073)
Z	4	4	4
d_{calcd} (g cm^{-3})	1.436	1.379	1.433
F(000)	1796	1700	1788
μ (mm^{-1})	0.319	0.321	0.321
no. of unique data	3897	3925	3772
no. of restraints	0	0	0
no. of parameters refined	293	279	306
goodness of fit on F^2	1.067	1.020	1.042
R1[a]	0.0609	0.0390	0.0570
wR2[b]	0.1651	0.0992	0.1562

[a] For data with $I > 2\sigma I$, $R1 = \sum||F_o| - |F_c|| / \sum|F_o|$. [b] For all data. $wR_2 = \{\sum[w(F_o^2 - F_c^2)^2] / \sum[w(F_o^2)^2]\}^{1/2}$.

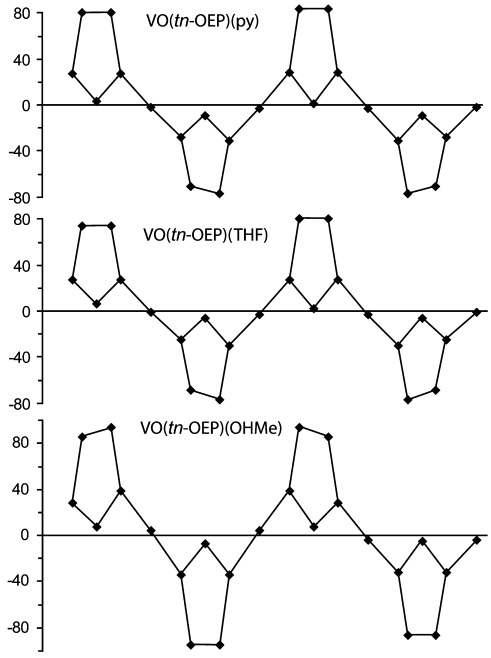

Figure 6. Diagrams comparing the out-of-plane displacements (units of 0.01 Å) of the porphyrin core atoms from the mean porphyrin plane for VO(*tn*-OEP)(py), VO(*tn*-OEP)(THF), and VO(*tn*-OEP)(OHMe).

distance is 2.424(3) Å, which is subject to the trans influence of the oxo oxygen. However, the methanolic carbon atom, C19, is disordered over two positions. Figure 5 shows the H-bonding interactions [O1···O6, 2.960(3) Å] between the methanolic hydrogen of one molecule and the oxo oxygen of the other molecule forming an infinite, linear chain in the packing diagram.

The porphyrin rings are highly distorted in all three molecules. This is shown in Figure 6 where the out-of-plane displacements in units of 0.01 Å of the core atoms are compared. The nomenclature that describes the types of distortions commonly observed in nonplanar porphyrins was originally suggested by Scheidt and Lee.[16] In a saddle conformation, alternate pyrrole rings tilt up and down with respect to the porphyrin mean plane (24 atoms), and the meso carbon atoms lie on the least-squares plane. In a ruffled conformation, alternate pyrrole rings twist clockwise or counterclockwise about the metal−nitrogen bond, and the meso carbon atoms move alternately above or below the least-squares plane of a 24-porphyrin atom core. As is evident from Figure 6, the ring distortions for all three complexes can be described as the purely saddle type with alternating displacement of the pyrrole rings below and above the mean porphyrin plane, while the pyrrole nitrogen and meso carbons are placed on the plane. The average displacements of the 24 atoms of the porphyrin core increase in the order of VO(*tn*-OEP)(THF) < VO(*tn*-OEP)(py) < VO(*tn*-OEP)(OHMe), and the average dihedral angles between a pyrrole ring and the mean least-squares plane of porphyrin are 18.9°, 19.7°, and 22.8° for VO(*tn*-OEP)(THF), VO(*tn*-OEP)(py), and VO(*tn*-OEP)(OHMe), respectively.

Table 3 shows the comparison of the structural and geometrical features between the six-coordinate VO(*tn*-OEP)(L) and the five-coordinate VO(OEP). All six-coordinate complexes reported here have stable V═O bonds, where the lengths vary in the narrow range of 1.592(3)−1.600(3) Å. The small difference in the V═O bond lengths for these complexes indicates that axial ligand coordination exerts only a small influence upon the Lewis acidity of the V(IV) center. However, the average V−Np distances are significantly smaller than the average 2.102(6) Å distance found for VO(OEP)[17d] or similar distances found for all other five-coordinate vanadyl porphyrins reported.[17] Thus, the shortening of the V−Np distance confirms the significant effects of axial coordination. In contrast, the addition of the axial ligand increases the M−Np distances for Ni(*tn*-OEP) and Zn(*tn*-

(16) Scheidt, W. R.; Lee, Y. J. *Struct. Bonding (Berlin, Ger.)* **1987**, *64*, 1.

Table 3. Selected Geometrical Parameters

	VO(*tn*-OEP)(py)	VO(*tn*-OEP)(THF)	VO(*tn*-OEP)(OHMe)	VO(OEP)[a]
V−N_p (Å)[b]	2.072(3)	2.073(3)	2.066(3)	2.102(6)
V−L_{ax} (Å)	2.492(3)	2.404(3)	2.424(3)	−
V═O (Å)	1.600(3)	1.592(3)	1.595(2)	1.620(2)
Δ^{V}_{4N} (Å)[c]	0.31	0.32	0.34	0.54
Δ^{V}_{24} (Å)[d]	0.34	0.33	0.35	0.59
Φ_{pyr} (deg)[e]	19.7	18.9	22.8	4.4
ΔC_m (Å)[f]	0.01	0.01	0.06	0.07
ΔC_β (Å)[f]	0.78	0.75	0.90	0.15
Δ_{24} (Å)[g]	0.37	0.35	0.43	0.07
core size (Å)	2.052	2.049	2.035	2.031

[a] Taken from ref17d. [b] Average distance. [c] Displacement of vanadium from the mean plane of four porphyrinic nitrogens. [d] Displacement of vanadium from the least-squares plane of porphyrin (24 atoms). [e] Average angle between the mean porphyrin plane (24 atoms) and the pyrrole rings. [f] Average displacement of the respective carbon atom from the four porphyrinic nitrogens. [g] Average displacement of the 24 atoms from the least-squares plane of the porphyrin.

OEP).[18] Porphyrin cores (center-to-nitrogen distances) also have been expanded slightly for VO(*tn*-OEP)(L) compared to those of the five-coordinate vanadyl porphyrins, which allows the vanadium atom to be more inplane (∼0.2 Å) as compared to the out-of-plane displacement of 0.54 Å observed in VO(OEP). Also, the axial V−N/O(L) distances are much longer because of the trans influence of the oxo oxygen, while V−O(L) distances are relatively shorter compared to V−N(L) distances. However, the vanadium atoms in the complexes are well-separated in the crystal lattice with the closest V···V separation being 9.745, 9.593, and 6.564 Å for VO(*tn*-OEP)(py), VO(*tn*-OEP)(THF), and VO(*tn*-OEP)(OHMe), respectively, which is consistent with noninteracting molecules.

The present study shows that the addition of strong electron-withdrawing nitro groups at the meso positions has a significant impact on the electronic and structural properties of metalloporphyrins, which have a marked effect on the reactivity of the central vanadyl ion. The successive addition of mononitro, dinitro, and trinitro substituents at the meso positions on the vanadyl octaethylporphyrins also results in axial ligand coordination in solution as seen by the bathochromic shifts of the UV−vis bands,[20] but all attempts to isolate them in the solid phase are futile, even in the presence of strong nitrogenous bases such as piperidine.[21] However, the addition of four nitro groups in the meso positions causes significant distortion of the porphyrin macrocycle, and its strong electron-withdrawing character has significantly enhanced the relative affinity of the vanadyl porphyrins for axial ligands, so much so that even the weak, σ-donating ligand, methanol, binds strongly enough to be isolable in the solid state. The effect of increasing distortion on the chemical reactivity with axial-ligating agents, which normally acts to lower the affinity, is overcome in the nitro-octaethylporphyrin series by the increasing electron depletion of the porphyrin ring as the number of nitro substituents increases. These results suggest that a significant electronic effect from the nitro substituent is transmitted to the central metal that increases the partial positive charge on vanadium leading to facile axial ligand coordination. Therefore, the axial ligand affinity is influenced by both electronic and conformational effects, which cannot be separated completely in this series.

The enhancement in the axial ligand affinity also was observed to some extent in the case of Ni(*tn*-OEP). For example, in piperidine both four- and six-coordinate complexes are observed for Ni(OEP), whereas only the six-coordinate species is present for Ni(*tn*-OEP).[18e] Also, Ni(II) porphyrins normally occur in the low-spin state ($S = 0$) when there are no axial ligands, but they yield the six-coordinate, high-spin Ni(*tn*-OEP)$(py)_2$ in the presence of pyridine, where the Ni−Np bond lengths [2.049(5) Å] are significantly elongated compared to similar bond lengths found in Ni(*tn*-OEP) [1.917(4) and 1.922(4) Å].[18a] In the case of Zn(*tn*-OEP), the addition of methanol did not yield the expected five-coordinate Zn^{II}(*tn*-OEP)(OHMe) species, but rather the polymeric compound of the general formula $\{Zn^{II}(tn\text{-OEP})\}_n$, where polymer formation was achieved via the utilization of nitro oxygen atoms as axial ligands to the metal center of neighboring porphyrins.[18c] However, a series of five-coordinate Zn^{II}(*tn*-OEP)(L) (where L is imidazole, 1-methylimidazole, 2-methylimidazole, etc.) were readily prepared by the addition of a nitrogenous base as the axial ligand (L), where the Zn−Np distances [2.084(6) Å when L is imidazole; 2.086(3) Å when L is 1-methylimidazole, etc.] are significantly elongated compared to similar distances [Zn−Np, 2.047(4) Å] found in $\{Zn(tn\text{-OEP})\}_n$.[18b] Similarly, the Co^{II}(*tn*-OEP) derivative also showed a polymeric complex $\{Co^{II}(tn\text{-OEP})\}_n$ isostructural to that described for $\{Zn^{II}(tn\text{-OEP})\}_n$,[18b] which also converts to monomeric Co^{II}(*tn*-OEP)$(py)_2$ in the presence of pyridine.[18b] In the case of Fe(*tn*-OEP)Cl, the addition of nitrogenous axial ligand L (L is pyridines, imidazoles, etc.) changes the metal oxidation states from the high-spin ferric to the low-spin ferrous state

(17) (a) Harada, R.; Okawa, H.; Kojima, T. *Inorg. Chim. Acta* **2005**, *358*, 489. (b) Duval, H.; Bulach, V.; Fischer, J.; Weiss, R. *Acta Crystallogr.* **1998**, *C54*, 1781. (c) Drew, M. G. B.; Mitchell, P. C. H.; Scott, C. E. *Inorg. Chim. Acta* **1984**, *82*, 63. (d) Molinaro, F. S.; Ibers, J. A. *Inorg. Chem.* **1976**, *15*, 2278.

(18) (a) Barkigia, K. M.; Renner, M. W.; Senge, M. O.; Fajer, J. *J. Phys. Chem. B* **2004**, *108*, 2173. (b) Senge, M. O. *J. Porphyrins Phthalocyanines* **1998**, *2*, 107. (c) Senge, M. O.; Smith, K. M. *J. Chem. Soc., Chem. Commun.* **1994**, 923. (d) Senge, M. O. *J. Chem. Soc., Dalton Trans.* **1993**, 3539. (e) Hobbs, J. D.; Majumder, S. A.; Luo, L.; Sickelsmith, G. A.; Quirke, J. M. E.; Medforth, C. J.; Smith, K. M.; Shelnutt, J. A. *J. Am. Chem. Soc.* **1994**, *116*, 3261.

(19) Patra, R.; Chaudhary, A.; Ghosh, S. K.; Rath, S. P. *Inorg. Chem.* **2008**, *47*, 8324.

(20) Axial ligand coordinations in solution for V(IV) derivatives of 5-mono-, 5,10-di-, and 5,10,15-tri-meso-nitro-substituted octaethyl porphyrins are observed by the bathochromic shifts of the UV−vis bands as shown. UV-vis in chloroform (λ_{max} at 295 K): for VO[(NO_2)OEP], 411, 538, and 577 nm; for VO[(NO_2)OEP](py), 426, 547, and 580 nm; for VO[$(NO_2)_2$OEP], 413, 540, and 579 nm; for VO[$(NO_2)_2$-OEP](py), 428, 551, and 587 nm; for VO[$(NO_2)_3$OEP], 417, 545, and 582 nm; and for VO[$(NO_2)_3$OEP](py), 432, 557, and 589 nm.

(21) Ghosh, S. K.; Rath, S. P. Unpublished results.

Table 4. Electrochemical Data

	oxidation		reduction		
complex	$E_{1/2}(1)$	$E_{1/2}(2)$	$E_{1/2}(1)$	$E_{1/2}(2)$	$E_{1/2}(3)$
VO(*tn*-OEP)[a]	1.39[e]	1.55[e]	−0.20 (110)[d]	−1.04 (110)[d]	−1.32[f]
VO(*tn*-OEP)(Py)[b]	1.34[e]	1.53[e]	−0.25 (110)[d]	−1.14 (100)[d]	−1.46 (80)[d]
VO(*tn*-OEP)(THF)[c]	−	1.50[e]	−0.17 (90)[d]	−1.06 (90)[d]	−1.35 (80)[d]

[a] Cyclic voltammogram in CH_2Cl_2. [b] Cyclic voltammogram in CH_2Cl_2 in the presence of 10% pyridine. [c] Cyclic voltammogram in tetrahydrofuran. [d] Half-wave potentials $E_{1/2} = (E_{pa} + E_{pc})/2$ (peak potential differences in mV in parentheses). [e] Irreversible oxidation processes, E_{pa}. [f] Irreversible reduction processes, E_{pc}.

immediately to form Fe(*tn*-OEP)$(L)_2$, while the additions of MeOH and H_2O as axial ligands produce high-spin ferric complexes of Fe(*tn*-OEP)(OHMe)Cl and Fe(*tn*-OEP)$(OH_2)_2^+$, respectively.[19] However, in the case of VO(*tn*-OEP)(L), the average V−Np distances are significantly smaller than similar distances found in the five-coordinate vanadyl porphyrins reported so far. The binding of L does not change the spin and oxidation states of the metal (V^{IV}, d^1-system), and thus the changes observed are truly the reflections of axial ligand coordination. In contrast, the addition of axial ligands increases the M−Np distances in the cases of Ni(*tn*-OEP) and Zn(*tn*-OEP).[18] These results can be useful for identifying the interaction of the vanadyl porphyrins with the biological targets in their reported involvement in potent insulinomimetic activity and in anti-HIV agents.

There is a report[13] of a six-coordinate, π-cation, radical complex, $[VO(OH_2)(OEP^{\bullet})]SbCl_6$, where the sixth position is occupied partially by a water molecule, with a partial occupancy of only 60%. However, it was proposed that metallo, π-cation derivatives display substantially enhanced affinity for aquo ligands relative to the ring neutral analogs, presumably because of the overall positive charge.[13] The V−O distances are 1.578(4) and 2.473(8) Å with oxo oxygen and axial water ligands, respectively, while the average V−Np bond distance is 2.063 Å. Although the average V−Np distances are very similar, the V−O(L) distance is relatively longer compared to similar distances observed in VO(*tn*-OEP)(OHMe) and VO(*tn*-OEP)(THF) reported here. Also, the vanadium atom is displaced from the mean porphyrin plane of the 24-atom core toward oxo oxygen by 0.46 Å in $[VO(OH_2)(OEP^{\bullet})]SbCl_6$, which is substantially longer than the average displacement of 0.32 Å observed in the authentic six-coordinate VO(*tn*-OEP)(L) containing highly distorted porphyrin macrocycles.

Cyclic Voltammetry. All of the complexes reported are redox active in solution, and the potentials are summarized in Table 4; a representative cyclic voltammogram is shown in Figure 7 for VO(*tn*-OEP)(THF).

Electrochemical data obtained from cyclic voltammetric studies reveal that VO(*tn*-OEP) in CH_2Cl_2 undergoes two one-electron oxidations at 1.39 and 1.55 V because of the formation of π-cation radical and dication, respectively, and three one-electron reductions at −0.20, −1.04, and −1.32 V. The first two reductions observed for VO(*tn*-OEP) are quasi-reversible due to the formation of the monoanion radical $V^{IV}O(tn\text{-}OEP^{\bullet})^-$ and the dianion $V^{IV}O(tn\text{-}OEP)^{2-}$, while the third irreversible reduction is assigned to a metal-centered process ($V^{IV} \rightarrow V^{III}$). In contrast, VO(OEP) shows two oxidation peaks at 0.88 and 1.29 V, and only one reduction peak at −1.37 V under the same experimental conditions. Therefore, it is easy to reduce VO(*tn*-OEP) by ∼1200 mV, whereas oxidations by ∼500 mV are difficult compared to those of nearly planar VO(OEP). The main features distinguishing VO(*tn*-OEP) from VO(OEP) are the severe macrocycle distortion and the presence of four electron-withdrawing nitro groups in the four meso positions. Published electrochemical data[22] on a variety of metalloporphyrins show that inducing distortion of the macrocycle will lead to an easier oxidation, while the addition of the electron-withdrawing groups will lead to a more difficult oxidation, which dominates in this series. Therefore, the addition of four NO_2 groups in the porphyrin macrocycle serves both to protect the reactive meso position from rapid oxidative attack and to stabilize the porphyrin and the metal against any oxidative degradation during the catalytic oxygenation process.

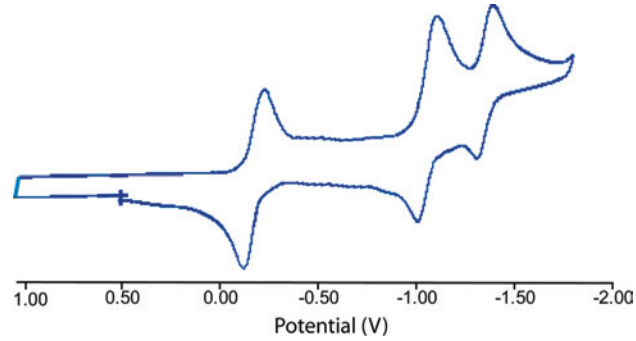

Figure 7. Portion of cyclic voltammogram for VO(*tn*-OEP)(THF) in THF (scan rate of 100 mV/s) with 0.1 M tetra(*n*-butyl)ammonium perchlorate as the supporting electrolyte. The reference electrode was Ag/AgCl.

Similar oxidations are also observed for VO(*tn*-OEP)(py) which are found at 1.34 and 1.53 V, whereas VO(*tn*-OEP)(THF) shows only one oxidation peak at 1.50 V. Thus, axial ligand binding to vanadyl porphyrins also leads to easier oxidation. Moreover, three one-electron reductions also are observed for VO(*tn*-OEP)(L) (Table 4). The first two reductions are quasi-reversible due to the formation of π-anion radical and dianion. The third reduction that is irreversible for VO(*tn*-OEP) becomes more negative and quasi-reversible for VO(*tn*-OEP)(py) and VO(*tn*-OEP)(THF) (Figure 7) and is assigned to a metal-centered process ($V^{IV} \rightarrow V^{III}$). Figures S2 and S3 (Supporting Information) show the cyclic voltammograms of VO(*tn*-OEP) and VO(*tn*-OEP)(py), respectively.

(22) (a) Kadish, K. M.; Caemelbecke, E. V.; Royal, G. In *The Porphyrin Handbook*; Kadish, K. M., Smith, K. M., Guilard, R., Eds.; Academic Press: New York, 2000; Vol. 8, p 1. (b) Kadish, K. M.; Royal, G.; Caemelbecke, E. V.; Gueletti, L. In *The Porphyrin Handbook*; Kadish, K. M., Smith, K. M., Guilard, R., Eds.; Academic Press: New York, 2000; Vol. 9, p 1.

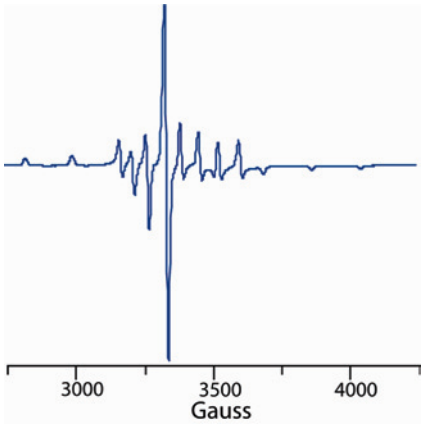

Figure 8. X-Band EPR spectrum of VO(*tn*-OEP)(THF) in THF at 120 K. EPR parameters: microwave frequency, 9.433 GHz; incident microwave power, 0.201 mW; modulation frequency, 100 kHz; modulation amplitude, 10.0 G; receiver gain, 1.0×10^3.

EPR Spectra. Solids and solutions of all the paramagnetic complexes reported here exhibit axial EPR spectra with well-resolved, ^{51}V, hyperfine lines at 120 K (Experimental Section); a representative EPR spectrum is shown in Figure 8 for VO(*tn*-OEP)(THF). The $g_{\|} < g_{\perp}$ and $A_{\|} \gg A_{\perp}$ relationships are normal for the axially compressed d^1_{xy} configuration. Similar EPR spectra are also observed for VO(*tn*-OEP)(py) and VO(*tn*-OEP)(OHMe) as shown in Figure S4 (Supporting Information).

Conclusions

In conclusion, we have presented a hitherto unknown family of six-coordinate vanadyl porphyrins incorporating axial ligand L isolated as VO(*tn*-OEP)(L) in the solid state for the first time and also structurally characterized. All earlier attempts to isolate such species were futile. In the UV−vis spectra, the porphyrin distortion is reflected in the red shift and the broadening of the Soret and Q-bands are relative to nearly planar VO(OEP). The solid-state magnetic measurements and their typical EPR spectra show the presence of a single, unpaired electron that is consistent with the V(IV) formulation. The V═O stretching frequency for VO(*tn*-OEP) occurs as a sharp, strong peak at 1008 cm^{-1}, consistent with five-coordinate vanadyl porphyrins, while VO(*tn*-OEP)(L) displays a strong band at lower wavenumbers. The downshift in ν(V═O) upon axial coordination increases with increasing donor strength of the axial ligands; for pyridine, the downshift is 30 cm^{-1}, while for THF and MeOH, the downshifts are nearly 18 cm^{-1}.

Porphyrin rings are highly distorted in all three molecules; the ring distortions can be described as the purely saddle type with alternating displacement of the pyrrole rings below and above the mean porphyrin plane, while the pyrrole nitrogen and meso carbons are placed on the plane. The introduction of four nitro groups into the meso positions of vanadyl octaethylporphyrin distorts the macrocycles severely and significantly enhances the affinity for the axial ligands, where even weak σ-donating ligands, such as MeOH, bind strongly enough to be isolable in the solid phase and that even under the offset effects of the macrocyclic distortions. Thus, axial ligand affinity is influenced by both the electronic and conformational effect for this series, which cannot be completely separated. X-ray structure determinations reveal that the V−Np distances are significantly shorter, and the porphyrin cores have been expanded because of axial ligand coordination. As a result, vanadium atoms are more inplane compared to those in the five-coordinate species. Also, the binding of axial ligands does not change the spin or oxidation states of the metal (V^{IV}, d^1-system), and thus, the changes observed are truly the reflections of axial ligand coordination. These results can be useful for identifying the interaction of the vanadyl porphyrins with the biological targets in their reported involvement in potent insulinomimetic activity and in anti-HIV agents.

Electrochemical data obtained from cyclic voltammetric studies reveal that the complexes are easier to reduce, but more difficult to oxidize, than the corresponding VO(OEP). Thus, the nitro groups serve both to protect the reactive meso position from rapid oxidative attack and to stabilize the porphyrin against oxidative degradation during any catalytic oxygenation process. The molecule undergoes two one-electron oxidations due to π-cation radical and dication formation and three one-electron reductions. The first two reductions are because of π-anion radical and dianion, while the third quasi-reversible reduction is assigned to the metal-centered process ($V^{IV} \rightarrow V^{III}$).

Experimental Section

Materials. Reagents and solvents were purchased from commercial sources and purified by standard procedures before use. Grade-I neutral alumina was used for column chromatography. H_2OEP[23] and tetranitrooctaethylporphyrin (*tn*-H_2OEP)[14] were prepared by literature methods.

Preparation of VO(*tn*-OEP). *tn*-H_2OEP (80 mg, 0.112 mmol) was dissolved in 80 mL of *N*,*N*-dimethylformamide and heated to reflux under a nitrogen atmosphere. $VOSO_4 \cdot H_2O$ (253 mg, 1 mmol) was added to the above solution, and reflux continued for 2.5 h. The reaction mixture was cooled to room temperature, and 80 mL of chloroform was added to it. The resulting mixture was then taken into a separating funnel and washed well with water. The organic layer was collected and dried over anhydrous Na_2SO_4, which was then evaporated to complete dryness. The product was purified by column chromatography on neutral alumina. The major fraction eluted with $CHCl_3$ was collected and evaporated to dryness to obtain a dark-purple solid. Yield: 60 mg (69%). Anal. Calcd (found): C, 55.46 (55.40); H, 5.14 (5.22); N, 14.38 (14.33). IR (KBr, ν_{max} cm^{-1}): 1008 (V═O). UV−vis ($CHCl_3$) [λ_{max}, nm (ϵ, M^{-1} cm^{-1})]: 427 (2.8×10^5), 556 (2.4×10^4), 596 (2.7×10^4). μ_{eff} (295 K): 1.76 μ_B. EPR data in DCM at 120 K: $g_{\|}$ ($A_{\|} \times 10^4$ cm^{-1}), 1.967 (174); $g_{\perp}$ ($A_{\perp} \times 10^4$ cm^{-1}), 1.973 (57).

Preparation of VO(*tn*-OEP)(py). To a benzene solution (5 mL) of VO(*tn*-OEP) (50 mg, 0.064 mmol) was added 0.5 mL of pyridine, and the mixture was stirred for 5 min. The resulting solution was then filtered and carefully layered with cyclohexane. On standing for 8−10 days in air, a dark-purple, crystalline solid was separated out that was collected by filtration, washed well with cyclohexane, and dried in a vacuum. Yield: 45 mg (81%). Anal. Calcd (found): C, 57.35 (57.31); H, 5.25 (5.32); N, 14.69 (14.62). IR (KBr, ν_{max}

(23) Sessler, L. J.; Mozaffari, A.; Johnson, M. R. *Org. Synth.* **1992**, *70*, 68.

cm^{-1}): 978 (V═O). UV−vis ($CHCl_3$ containing 10% pyridine) [λ_{max}, nm (ϵ, M^{-1} cm^{-1})]: 376 (9.9×10^4), 435 (2.7×10^5), 565 (3.2×10^4), 590 (2.2×10^4). μ_{eff} (295 K): 1.74 μ_B. EPR data in pyridine at 120 K: $g_{\|}$ ($A_{\|} \times 10^4$ cm^{-1}), 1.967 (175); $g_{\perp}$ ($A_{\perp} \times 10^4$ cm^{-1}), 1.975 (58).

Preparation of VO(*tn*-OEP)(THF). VO(*tn*-OEP) (50 mg, 0.064 mmol) was dissolved in 5 mL of tetrahydrofuran and stirred for 5 min to produce a clear solution that was then filtered to remove any solid residue. The filtrate collected was carefully layered with cyclohexane. On standing for 6−7 days in air, a dark-purple, crystalline solid was formed that was isolated by filtration, washed with cyclohexane, and dried in a vacuum. Yield: 43 mg (79%). Anal. Calcd (found): C, 56.41 (56.37); H, 5.64 (5.70); N, 13.16 (13.11). IR (KBr, ν_{max} cm^{-1}): 990 (V═O). UV−vis ($CHCl_3$ containing 10% THF) [λ_{max}, nm (ϵ, M^{-1} cm^{-1})]: 378 (9.0×10^4), 431 (2.7×10^5), 559 (2.9×10^4), 588 (2.1×10^4). μ_{eff} (295 K): 1.78 μ_B. EPR data in THF at 120 K: $g_{\|}$ ($A_{\|} \times 10^4$ cm^{-1}), 1.967 (176); $g_{\perp}$ ($A_{\perp} \times 10^4$ cm^{-1}), 1.978 (57).

Preparation of VO(*tn*-OEP)(OHMe). A 50 mg (0.064 mmol) sample of VO(*tn*-OEP) was dissolved in 5 mL of benzene and stirred for 5 min. The solution was filtered to remove any solid residue and then carefully layered with methanol and kept for slow diffusion in air. On standing for 7−8 days, a dark-purple, crystalline solid appeared that was then collected by filtration, washed well with methanol, and dried in a vacuum. Yield: 44 mg (85%). Anal. Calcd (found): C, 54.75 (54.72); H, 5.43 (5.50); N, 13.81 (13.83). IR (KBr, ν_{max} cm^{-1}): 989 (V═O); 3438 (br, OH). UV−vis ($CHCl_3$ containing 10% MeOH) [λ_{max}, nm (ϵ, M^{-1} cm^{-1})]: 375 (9.0×10^4), 432 (2.7×10^5), 559 (3.2×10^4), 589 (2.1×10^4). μ_{eff} (295 K): 1.71 μ_B. EPR data in MeOH at 120 K: $g_{\|}$ ($A_{\|} \times 10^4$ cm^{-1}), 1.967 (176); $g_{\perp}$ ($A_{\perp} \times 10^4$ cm^{-1}), 1.976 (59).

Instrumentation. UV−vis spectra were recorded on a Perkin-Elmer UV−vis spectrometer. Elemental (C, H, and N) analyses were performed on a Perkin-Elmer 2400II elemental analyzer. Infrared spectra were recorded in the range of 4000−400 cm^{-1} on a Vertex 70 Bruker spectrophotometer on KBr pellets. Electron paramagnetic resonance spectra were obtained on a Bruker EMX EPR spectrometer. Magnetic susceptibility data were collected using a Quantum Design MPMS SQUID magnetometer at room temperature. Cyclic voltammetric studies were performed on a BAS Epsilon electrochemical workstation using 0.1 M tetra-*n*-butylammoniumperchlorate (TBAP) as the supporting electrolyte. The reference electrode was Ag/AgCl, and the concentrations of the compounds were used on the order of 10^{-3} M. The ferrocene/ferrocenium couple occurs at $E_{1/2} = +0.45$ (65) V versus Ag/AgCl under the same experimental conditions.

Structure Solution and Refinement. Crystals were coated with light hydrocarbon oil and mounted in the 100 K dinitrogen stream of a Bruker SMART APEX CCD diffractometer equipped with CRYO Industries low-temperature apparatus, and intensity data were collected using graphite-monochromated Mo Kα radiation (λ = 0.71073 Å). The data integration and reduction were processed with SAINT[24] software. An absorption correction was applied.[25] Structures were solved by the direct method using SHELXS-97 and were refined on F^2 with the full-matrix least-squares technique using the SHELXL-97[26] program package. Non-hydrogen atoms were refined anisotropically. In the refinement, hydrogens were treated as riding atoms using SHELXL default parameters. Crystal data are given in Table 2.

Acknowledgment. We thank the Council of Scientific and Industrial Research (CSIR), India, for financial support, and the Indian Institute of Technolgy, Kanpur, for the infrastructural facility. S.K.G. and R.P. thank CSIR, India, for their fellowship. The authors also thank Prof. Marilyn M. Olmstead for valuable advice in a crystallographic problem.

Supporting Information Available: UV−vis spectra for all complexes (Figure S1), cyclic voltammograms of VO(*tn*-OEP) (Figure S2) and VO(*tn*-OEP)(py) (Figure S3), EPR spectrum of VO(*tn*-OEP)(py) and VO(*tn*-OEP)(OHMe) at 120 K (Figure S4), and X-ray crystallographic details in CIF format for VO(*tn*-OEP)(py), VO(*tn*-OEP)(THF), and VO(*tn*-OEP)(OHMe). This material is available free of charge via the Internet at http://pubs.acs.org.

IC800714W

(24) *SAINT*+, version 6.02; Bruker AXS: Madison, WI, 1999.
(25) *SADABS*; Bruker AXS: Madison, WI, 2007.
(26) Sheldrick, G. M. *Acta Crystallogr.* **2008**, *A64*, 112.